

# Emergence of non-ergodic multifractal quantum states in geometrical fractals

Fabio Salvati,\* Mikhail I. Katsnelson, and Andrey A. Bagrov

*Institute for Molecules and Materials, Radboud University,  
Heijendaalseweg 135, 6525 AJ Nijmegen, The Netherlands*

Eigenstate multifractality, a hallmark of non-interacting disordered metals which can potentially be observed in many-body localized states as well, is characterized by anomalous slow dynamics and appears relevant for many areas of quantum physics from measurement-driven systems to superconductivity. We propose a novel approach to achieve non-ergodic multifractal (NEM) states without disorder by iteratively introducing defects into a crystal lattice, reshaping it from a plain structure into fractal geometry. By comprehensive analysis of the Sierpiński gasket case, we find a robust evidence of the emergence of NEM states that go beyond the conventional classification of quantum states and designate new pathways for quantum transport studies. We discuss potential experimental signatures of these states.

## INTRODUCTION

Since the discovery of Anderson's localization paradigm [1], there has been a significant interest in critical phenomena that transcend the traditional dichotomy of extended and localized states. Among these, a class of novel states, commonly referred to as non-ergodic multifractal states (NEMs) [2, 3], has attracted particular attention. NEMs occupy a finite volume of the system but their support is a set of points that, in the thermodynamic limit, has a zero measure, challenging the conventional ideas of how a quantum state can be distributed in space. The concept of multifractality finds broad applications in a wide range of domains of science and engineering, including fluid dynamics [4], topography [5], finance [6], physiology [7], and epidemic modeling [8]. It also inspired advancements in machine learning, granting unexplored settings to incorporate larger hierarchical depth and achieve stable and robust prediction performances [9, 10]. In condensed matter physics, the concept of NEM is strictly connected to the singular continuous nature of the spectrum [11–13] and the critical scaling behavior [14] observed at phase transitions, which give rise to anomalous subdiffusive dynamics [15, 16] and make NEM particularly intriguing in the context of quantum transport. Additionally, they exhibit sublinear growth of entanglement entropy [17], defying the standard formulation of eigenstate thermalization hypothesis [18]. These attributes are essential for understanding quantum coherence of eigenstates [19] and many-body localization phenomena [20, 21]. Moreover, it is conjectured that multifractality can enhance electron-electron interactions leading to elevated critical temperature in superconductors [22, 23].

Incommensurate potentials in one-dimensional systems [24, 25] and randomness in higher-dimensional systems [26–28] are genuine mechanisms to induce disorder causing the emergence of NEMs in quantum systems. However, their direct experimental observations remain problematic due to finite-size effects and the dependence on fine-tuning, posing considerable difficulties for further exploration of NEMs. In this work, we propose an approach to generating such states. Rather than relying on randomness to induce disorder, we introduce a model that generates multifractal states through geometric manipulation by placing substitutional point-like defects in a regular lattice. Specifically, we focus on the case when these defects are arranged to transform the parental lattice into a regular fractal geometry [29]. In the past few years, properties of artificial quantum fractals structures have been systematically explored both experimentally and theoretically [30–40]. Here, our aim is to demonstrate how the self-similar structure and non-integer dimensionality of fractals offer a natural framework for designing and studying multifractal eigenstates. We consider single-particle quantum mechanics of a tight-binding model on a Sierpiński Gasket (SG), and through a comprehensive numerical analysis we demonstrate multiple crossovers between extended states and distinct stages of multifractality in the model spectrum. By calculating the fractal dimensions, we identify energy intervals where transitions to multifractal behavior occur. By examining the singularity spectrum, we gain deeper insights into the multifractal nature of individual states, unveiling a variety of behaviors including metallic and insulating NEM. In addition, we observe formation of clusters in the spatial structure of the wavefunctions that we classify as compact localized states (CLSs) [41, 42], which emerge as localized modes on the lattice subsets due to destructive interference on resonant groups of sites.

Recent advancements in spin-resolved scanning tunneling microscopy (STM) and spectroscopy techniques [43, 44] have enabled precise control over quantum states in low-dimensional structures, where quantum confinement is strong.

---

\* fabio.salvati@ru.nl

Having this in mind, we also present a detailed numerical analysis of the density-density correlation functions, which can be directly observed in such experiments. By pinpointing the regions where crossovers to NEMs occur, we compute these correlators and show that they exhibit a power-law decay combined with irregular oscillations and revivals in the frequency domain caused by self-similarity of the underlying fractal structure. Overall, these features form a robust criterion to unambiguously distinguish NEMs from both extended and localized states. Yet another verifiable aspect of multifractal systems is the mutual avoidance of eigenstates [45] at large energy separations, offering additional mechanisms by which they stand apart from quantum systems without NEMs in the spectrum.

While this study is of a purely fundamental theoretical nature, one can hope that NEMs, due to their unconventional properties, can be practically useful in certain contexts like quantum control or superconductivity. Hence, a key question here is: can multifractal states demonstrate sufficient resilience to perturbations to support their practical use? To address this, we introduce additional randomly distributed geometric defects into the system. Our analysis shows that, qualitatively, NEMs exhibit robustness in the presence of such perturbations. What is even more compelling, CLSs react to manipulation of individual atoms in a very structured and symmetric way, possibly opening an opportunity to use them for delicate control in quantum systems.

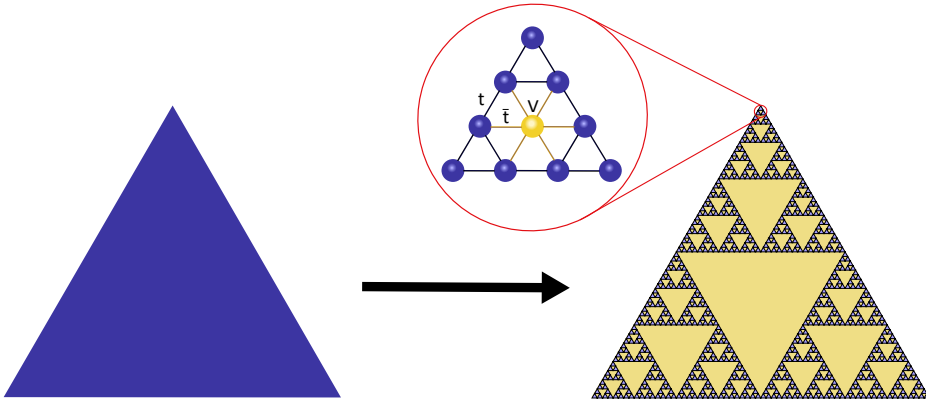


FIG. 1. Transformation of regular geometry into a fractal structure: from triangular lattice (left) into a sixth generation Sierpiński gasket (right). Zoom-in: the elementary building block of the SG with a substitutional defect (yellow dot). The hopping between regular sites is  $t$ . The defect has on-site potential  $V$ , and the corresponding hoppings connecting it with the rest of the lattice are  $\bar{t} \ll t \ll V$ .

## RESULTS

### Model

Our starting point is a uniform triangular lattice  $\mathcal{L}$  containing  $N$  sites, each uniquely indexed. The corresponding tight-binding Hamiltonian is a matrix of dimensions  $N \times N$ . Due to the uniform geometry of the lattice and assuming that the hopping occurs only between the nearest neighbors, we set the elements of the Hamiltonian to  $t_{ij} = t = 1$  for neighboring sites  $i$  and  $j$ . The diagonal elements are initially set to zero, neglecting any on-site potential at this stage.

The transformation of the triangular lattice into a SG is achieved by iterative placement of defects into regions corresponding to voids in the fractal structure up to the desired generation, as shown in Fig. (1). The set of defect sites forms a subset of the original lattice denoted as  $\mathcal{B} \subset \mathcal{L}$ . Each defect, located at position  $r_i$ , is modeled as a delta-peaked potential:  $V_i = V \delta(r - r_i)$  with strength  $V$  significantly larger than any other characteristic energy scale in the system. To make the defects act as voids of the fractal, the hoppings involving defect sites are rescaled to  $\bar{t} \ll t \ll V$ . The Hamiltonian reads:

$$H = \sum_{\substack{\langle i,j \rangle \\ i,j \notin \mathcal{B}}} t c_i^\dagger c_j + \sum_{i \in \mathcal{B}} V c_i^\dagger c_i + \sum_{\substack{\langle i,j \rangle \\ i \in \mathcal{B}}} \bar{t} c_i^\dagger c_j + h.c. \quad (1)$$

We then employ exact diagonalization to determine the complete set of eigenvalues and eigenvectors of the resulting single-particle Hamiltonian, with open boundary conditions applied. For the results presented here, the interaction

parameters are set to  $\bar{t} = 10^{-9}$ ,  $t = 1$ , and  $V = 10^4$ . We emphasize that this particular choice of parameters is not unique. Any set of values satisfying the inequality  $\bar{t} \ll t \ll V$  is equally valid and would lead to similar qualitative outcomes.

### Eigenstates statistics

The degree of delocalization in a system can be probed by examining the structure of its eigenstates in a given basis. A common approach [46, 47] derived from the box-counting method [2, 14] is to analyze the asymptotic scaling properties of moments of order  $q$  of the wavefunction  $\Phi$  with the number of sites  $N$ :

$$\sum_{i=1}^N |\langle i | \Phi \rangle|^{2q} \sim N^{-(q-1)D_q}, \quad (2)$$

where  $D_q$  are known as the fractal dimensions, and  $\{|i\rangle\}$  form the Hilbert space basis. While Eq.(2) holds in any basis, in what follows we will be using basis of localized states, with  $|i\rangle$  wavefunction being fully concentrated at site  $i$ . In metallic phases, eigenfunctions are extended with typical amplitude at site  $i$  scaling inversely with the whole system volume. This corresponds to fractal dimension  $D_q = 1$  indicating ergodic and delocalized states. In contrast, in insulating phases, the fractal dimensions  $D_q \rightarrow 0$ , representing localized states with the amplitude being inversely proportional to the localization volume. In the critical regime, the states occupy only a vanishing fraction of the total Hilbert space [48], their fractal dimensions lie in the range  $0 < D_q < 1$ , and, moreover, exhibit non-trivial dependence on  $q$ , highlighting their non-ergodic, multifractal nature. In Fig. (2), we show how fractal dimension  $D_2$  - the second momentum with  $q = 2$  - varies across the complete set of eigenstates of the tight-binding model on the sixth generation of SG.

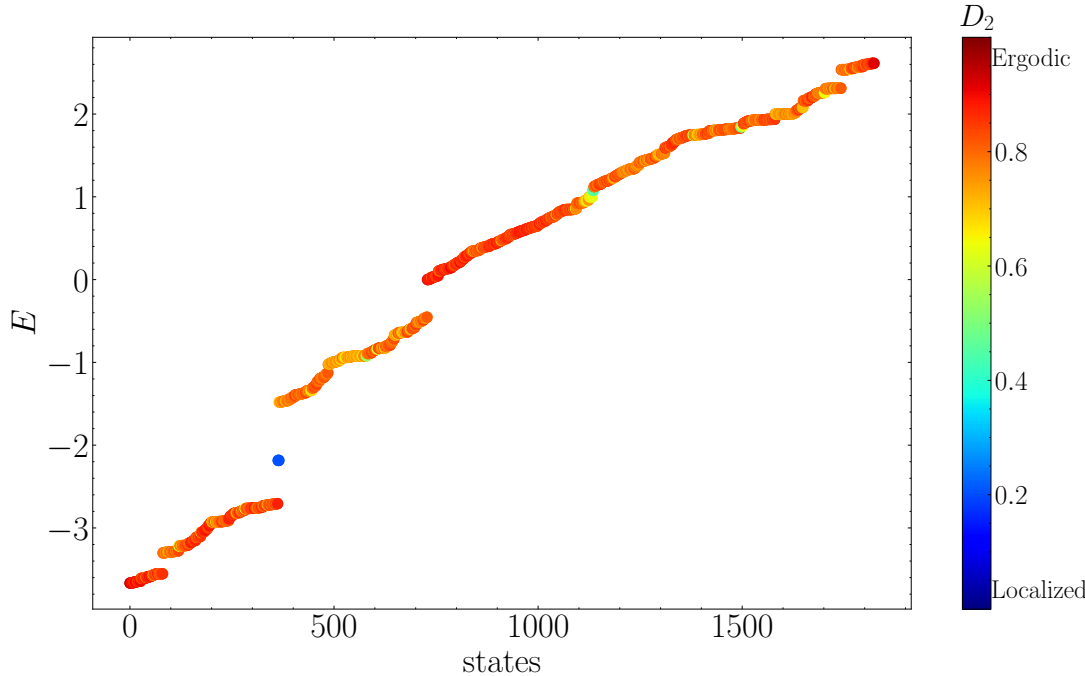


FIG. 2. Energy spectrum of the tight-binding model on the sixth generation of the Sierpiński Gasket. The color map show the fractal dimension  $D_2$  of each eigenstate. Multiple crossovers from extended states to NEMs are observed, with the only transition to localization occurring at  $E = -2.184$ .

The ground state and the first excited states have  $D_2 \geq 0.90$ , which is close to the expected values for extended states in finite size systems with open boundary conditions. As energy increases, however, the majority of states display significant deviations from the typical fractal dimension values associated with extended states. Surprisingly, the system almost never enters the localized regime, with the only exception of state with energy  $E = -2.184$ . Pronounced deviations of  $D_2$  from its limiting cases serve as one of indicators of the possible emergence of NEMs.

They are especially large near the spectral gaps and degenerate states, where the influence of the self-similar geometry plays a key role.

The next step is to employ a more refined measure of multifractality – the singularity spectrum  $f(\alpha)$ , a dual measure of the fractal dimensions (see Methods) with which one can assess the strength of multifractality of a single NEM. In Fig. (3), we present some case studies. The ground state ( $E = -3.666$ ), represented by the red curve, displays a narrow distribution peaked at  $\alpha = 1$ , close to the shape typical for an ideal extended state, as produced, for instance, by a Gaussian Orthogonal Ensemble (thick black line). On the other hand, the singularity spectrum represented with the blue curve for  $E = -2.184$  is distributed across a large domain of  $\alpha$  values and has its maximum shifted far away from  $\alpha = 1$ , as compared to the extended state. As anticipated already from its vanishingly small fractal dimension  $D_2$ , this picture closely resembles the case of an ideal localized state with infinite span of  $f(\alpha)$ . While the singularity spectrum at  $\alpha = 0$  does not reach zero here, as it should for strictly localized states in the thermodynamic limit, scaling analysis of the fifth and sixth generations of the gasket (see Supplemental Material) suggest a convergence trend. While finite-size scaling corrections likely affect these results, this evaluation is consistent with complementary indicators, including the two-point correlation function and the amplitude profiles, all of which support the interpretation of this state as localized. Finally, the yellow curve depicts the singularity spectrum of one of the NEM degenerate states at  $E = 1.847$ . Its parabolic shape, as well as the finite width and the apex shifted to  $\alpha > 1$  remain consistent under size scaling as shown in the Supplemental Material, aligning well with the previous predictions [2].

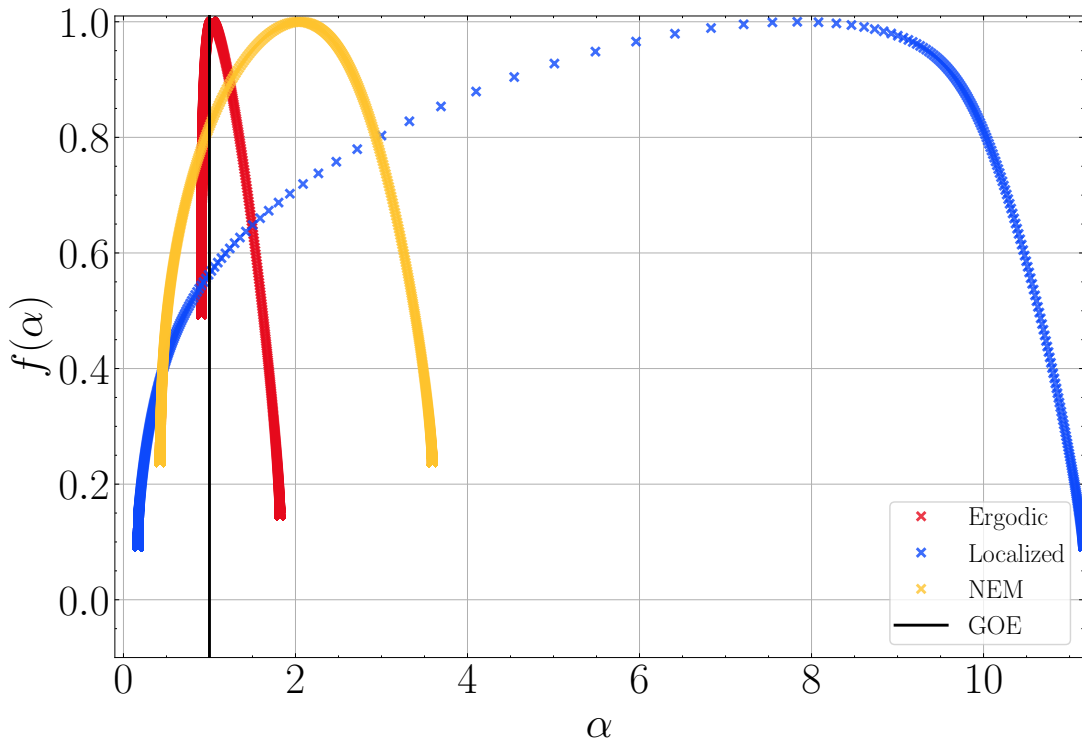


FIG. 3. Singularity spectrum of different states on the Sierpiński Gasket: representative cases of extended ( $E = -3.666$ , red), localized ( $E = -2.184$ , blue), and multifractal ( $E = 1.847$ , yellow) states are analyzed and compared with the Gaussian Orthogonal Ensemble (GOE), which serves as a reference for an ideal extended state. The differences in behavior can be inferred from both the position of the peak and the width of the curve.

Using these exemplary cases as a benchmark, one can examine the distribution of the singularity spectrum for different groups of eigenstates and acknowledge the emergence of different degrees of multifractality. NEMs can be not very pronounced, and their singularity spectrum can retain features of metallic or insulating phases [45, 49]. For such “mildy” multifractal states, the shift of the maximum of  $f(\alpha)$  may be minor, or its parabolic shape may be distorted, along with other anomalous behaviors known as termination or freezing [2]. One distinct class of states, neither extended nor localized in a rigorous sense, is observed for certain integer energy values. Though these states have a fractal dimension typical for NEMs, their singularity spectra do not abide by the conventional classification. As one can see from Fig. (4), the left branches of the  $f(\alpha)$  curves for these states are primarily concentrated around its maximum (like for the metallic states), while the right branches extend in a manner similar to that of the insulating

states. This suggests that these states exhibit a form of localization, albeit not restricted to a few sites in a single region. Despite coexistence of several regions of localization, we still refer to them as compact localized states (CLS) [41]. The emergence of CLS can be attributed to the interplay of hidden symmetries and destructive interference at resonant sites located along the reflection axes—characteristics inherent to the underlying fractal geometry, as visualized in the amplitude profiles (see the Supplemental Material). In fractal geometries, CLSs were first identified and numerically characterized in [50].

Other examples of multifractal states are presented in the Supplemental Material. Some of them have spatial structures analogous to the bulk and edge modes observed in fractal geometries [35, 51].

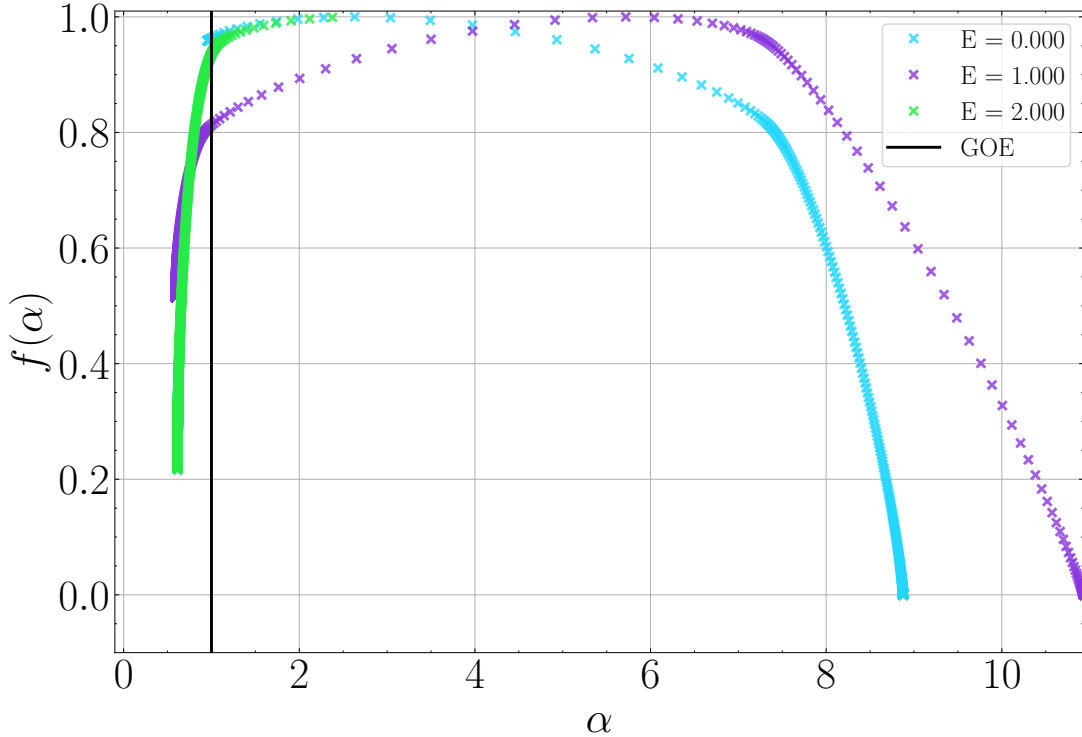


FIG. 4. Singularity spectrum for the Sierpiński Gasket: representative cases of compact localized states. While a CLS with a single cluster of non-zero  $|\psi|^2$  would exhibit behavior akin to a standard localized state, the coexistence of several clusters causes the left side of the  $f(\alpha)$  curve to concentrate densely around the GOE peak, with its density reflecting the number of isolated regions within the CLS. Further analysis of such states can be found in Supplemental Material.

We further expand upon our findings by probing the density-density correlators that encode for the overlap between eigenstates and serve as an additional tool to discriminate the NEMs, particularly at critical points when the correlator  $\mathcal{F}(\omega, E)$  decays as a power law (see Methods). Fig. (5) illustrates the behavior of  $\mathcal{F}(\omega, E)$  for the previously selected representatives of ergodic, localized and NEM states. As predicted by theory, the two-points correlator for the extended (red curve) and localized (blue curve) states exhibits a broad plateau across several orders of  $\omega$ . The intensity of the correlator reflects the degree of eigenstates overlap: it is low for extended states that share minimal information across a wide spatial region, and high for localized states that are concentrated in a confined region. However, in this particular case of localization, the plateau is especially pronounced, and from the amplitude profile of the state (see the Supplemental Material), it is evident that localization occurs within a single region, though with a slower decay. This suggests that localization is algebraic, rather than of the Anderson type. At large values of energy separation  $\omega$ , the correlator for both extended and localized states approaches the uncorrelated regime,  $\mathcal{F}(\omega, E) = 1$ , as marked by the typical GOE statistics. The NEM state (yellow curve) qualitatively behaves as expected, displaying a shorter plateau followed by a power-law decay towards the uncorrelated regime as  $\mathcal{F}(\omega, E) \sim (\omega/E_{Th})^{-\mu}$ . The exponent  $\mu$  and the Thouless energy  $E_{Th}$  are model-dependent and, unlike in disordered quantum systems, the lack of variable parameters in our Hamiltonian makes a possible analytic fit difficult. Notably, the density-density correlator behavior at higher frequencies is marked by pronounced oscillations with clear revivals and dips below the uncorrelated limit. This non-trivial behavior signals the presence of anomalies, reminiscent of effects observed in certain disordered quantum systems stemming from random matrix theory [52, 53]. In our model, these oscillations arise from the

competition between the eigenstate avoidance and the resonant states interference driven by the self-similar structure of the Sierpinski Gasket (SG). As shown in [45], the eigenstates avoidance is responsible for dips in  $\mathcal{F}(\omega, E)$  falling below the uncorrelated limit. Such dips indicate that, when a state predominantly occupies a site  $r$ , this site is likely to be vacant for other states: a behavior that is known as eigenstates stratification. On the other hand, revivals are not typical for randomly disordered systems and specific only for the considered case of regular fractal geometry.

Given that genuine multifractality should persist across different scales, we examine the scaling of correlator  $\mathcal{F}(\omega, E)$  with respect to system size  $N$  (see Fig. (6)) by computing it for subsequent generations of SG. The rescaled correlator  $\mathcal{F}(\omega, E)/N^{(1-D_2)}$  for the multifractal state at  $E = 1.847$ , shows remarkable consistency across different generations of the SG. The extent of the plateau and the locations of peaks and dips remain unchanged. Aside from minor finite-size corrections affecting the curve heights, the overall qualitative agreement is nearly perfect.

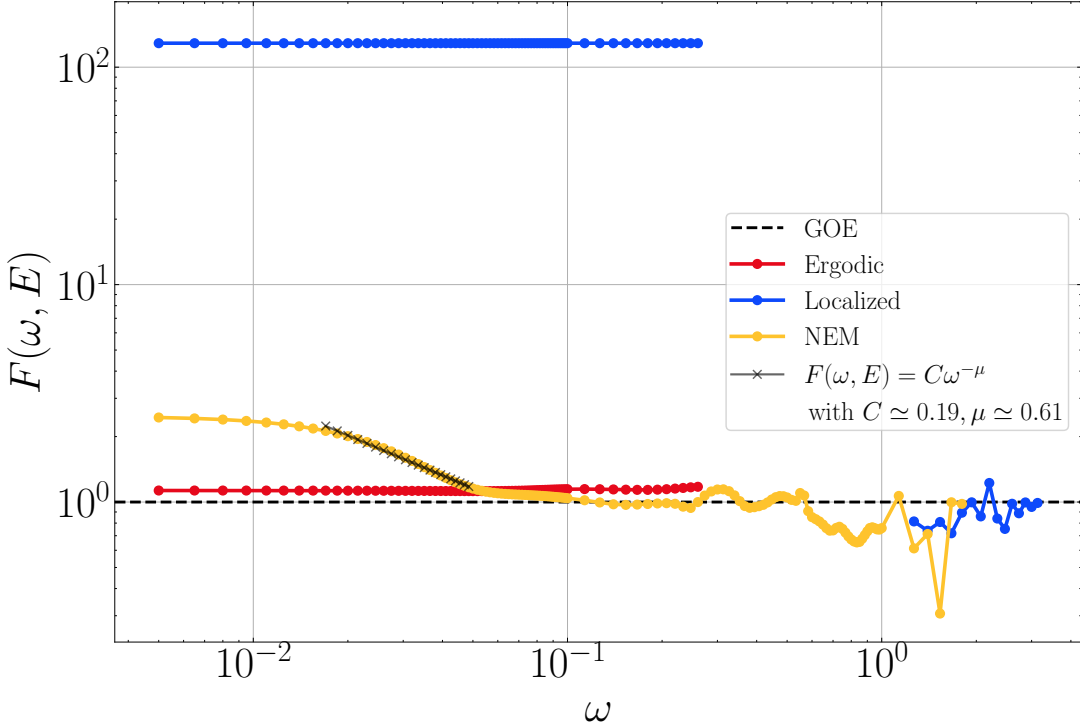


FIG. 5. Frequency correlator  $\mathcal{F}(\omega, E)$  for three characteristic cases: extended ( $E = -3.666$ , red), localized ( $E = -2.184$ , blue), and multifractal ( $E = 1.847$ , yellow). The ideal case of uncorrelated systems as described by the Gaussian Orthogonal Ensemble (GOE) is represented by the dashed black line. A broad plateau at small values of energy separation  $\omega$  is a hallmark of both extended and localized states, indicating non-vanishing correlations. In contrast, NEMs exhibit only a narrow plateau, which diminishes to a singular point in the thermodynamic limit, followed by a power-law decay highlighted with the black crosses. At larger values of  $\omega$ , only NEMs display revivals of the correlator, alongside a stratification phenomenon (in the Supplemental Material, examples with more pronounced revivals are presented). According to theory, the transition between phases at small and large energy separations should occur smoothly. However, in our simulations, discontinuities can appear in the correlator for both extended and localized states within the interval  $10^{-1} < \omega < 10$  due to numerically zero denominators in the computation of the density of states. Lines are guide to eye.

### Robustness and quantum control

So far, we have considered the case of a clear fractal structure. In reality, random defects existing on top of the regular fractal lattice will be likely unavoidable. Damaging the regular self-similar pattern of the fractal structure could trivially drive the NEMs of the original system towards a localized phase, and this needs to be analyzed.

In Fig. (7), we show the fractal dimension  $D_2$  for the set of eigenstates of the SG lattice in the presence of a number of additional random defects. One can see a clear general tendency for the NEMs to retain their multifractal nature, with  $D_2$  remaining distinct from the limiting case of localized states even for a large number of introduced defects. While individual NEMs may not exhibit robustness to disorder in a strict sense, the latent symmetries of the SG hierarchical structure act to prevent a full transition to localization, preserving the overall multifractal regime.

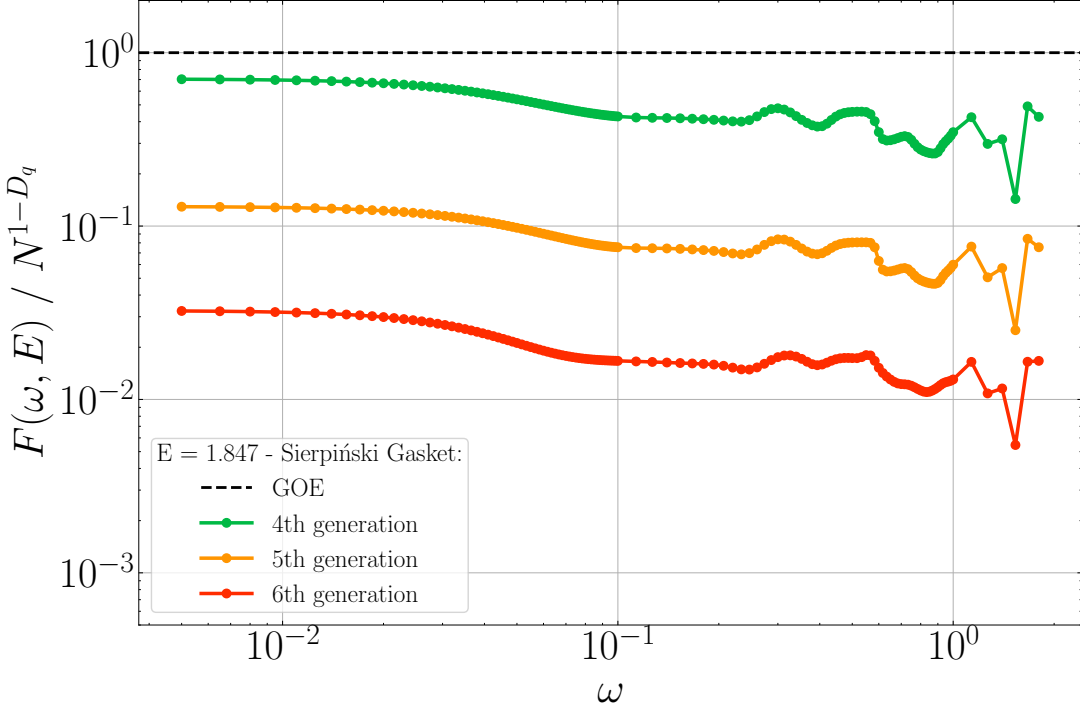


FIG. 6. Rescaled frequency correlator  $\mathcal{F}(\omega, E) / N^{(1-D_2)}$  for the NEM at energy  $E = 1.847$  shown for different generations of the Sierpiński Gasket. The Gaussian Orthogonal Ensemble, dashed black line, serves as the reference to an ideal uncorrelated system. The curves corresponding to different generations exhibit consistent behavior highlighting the scale-invariant properties of the NEM state. Lines are guide to eye.

The closing of gaps and the lifting of degeneracies reduce the average fractal dimension, yet the eigenstates of the system continuously reorganize themselves through resonances and stratification. This reorganization enables the NEMs to adapt, exploiting new patterns of multifractality that persist across different scales. Upon the introduction of additional defects, a broader spectrum of multifractal behaviors is observed, ranging from extended to insulating multifractal phases before an eventual transition to localization becomes inevitable.

The overall tendency of NEMs to persist upon introducing random defects can be complemented with a more detailed analysis of spatial structure of a specific state. In particular, compact localized states (CLSs) are of special interest due to their promise for applications to quantum information storage and transfer [42, 54]. As an illustrative example, we consider a state hosted by the sixth generation the SG lattice, Fig. (8), that can be created using atomic quantum simulators [44, 55]. By tuning the voltage to align the energy level with the CLS formation at  $E = 1.000$ , one can observe a nine-fold degenerate CLS exhibiting non-zero wavefunction amplitude solely in several isolated regions adjacent to the internal edges of the fourth level of the SG, Fig. (8a). The isolated clusters of the wavefunction intensity of CLSs remain unchanged unless perturbations directly affect the specific lattice sites on which these clusters have their support. At the same time, if defects are systematically introduced on sites within each cluster, the degeneracy of the state is lifted, and the wavefunction amplitude is redistributed among the remaining clusters without involving the other non-resonant sites Fig. (8b-d), allowing for targeted controlled manipulation of the wavefunction profile and offering a potential for accurate quantum control. As we show in the Supplemental Material, even if a larger number of random defects are introduced, and all the major clusters are destroyed, these disruptions lead to formation of new quantum interference patterns, wherein the information from a destroyed cluster stabilizes around lower levels of hierarchy of the fractal, which again results in formation of CLSs.

## DISCUSSION

With this work, we continue the research line of studying quantum phenomena in artificial fractal geometries, specifically focusing on the case of the Sierpiński gasket. We have shown that in clean fractal, without any added randomness, non-ergodic multifractal states naturally emerge, complementing the prior studies on wavefunction localization [35], quantum transport [16], and eigenstate statistics in fractals, and fractal energy spectra [32, 56]. We

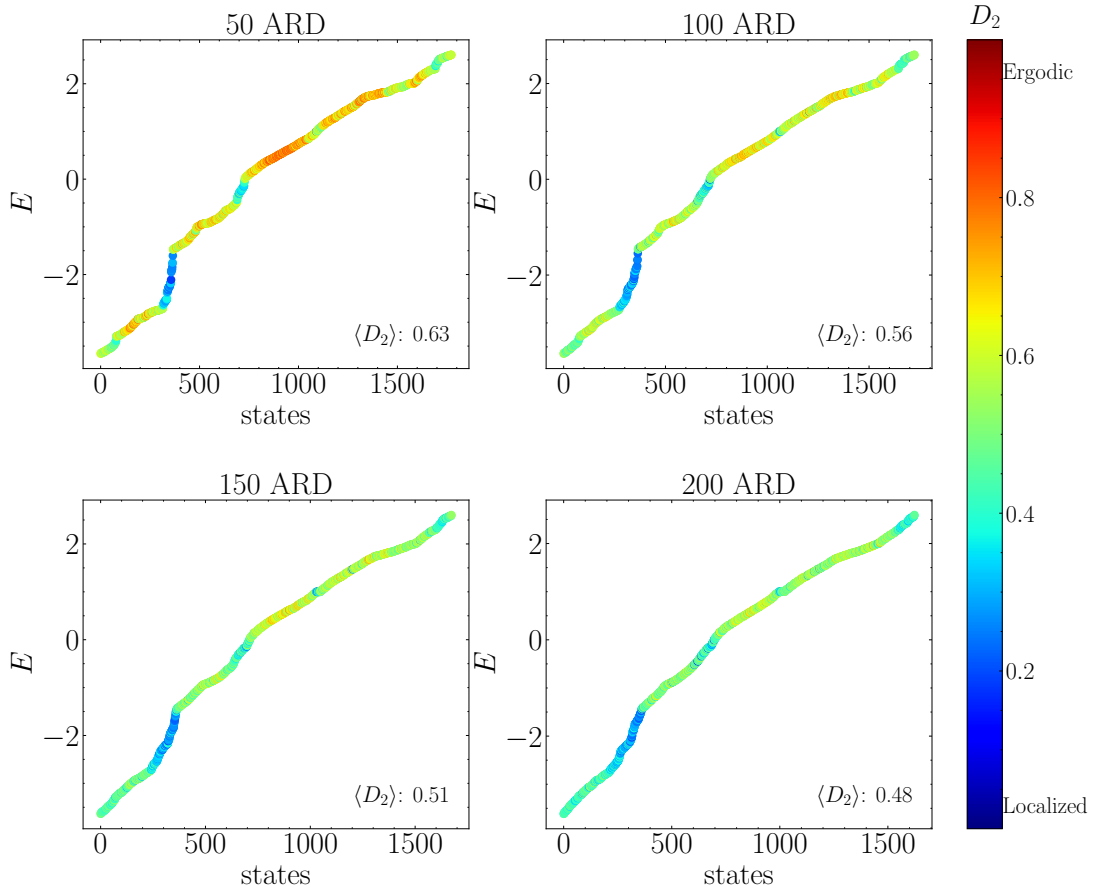


FIG. 7. Energy spectrum of the single-particle tight-binding model on the sixth generation of SG with additional random defects (ARD). Configurations with 50, 100, 150 and 200 ARD are analysed. The color indicates the fractal dimension  $D_2$  of each eigenstate. In the lower right corner of each subplot, the average of the fractal dimensions  $\langle D_2 \rangle$  over the spectrum is displayed, quantifying the tendency to localization as the number of defects increase.

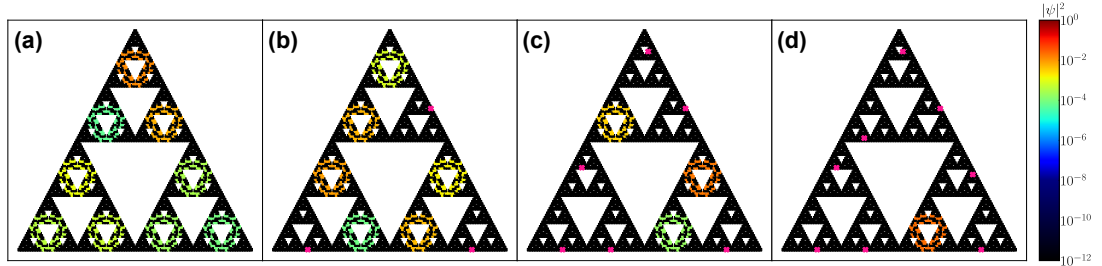


FIG. 8. Amplitude profile of the compact localised state at energy level  $E = 1.000$ . Profile (a) in the original model without defects, and (b-d) with additional defects (marked by pink crosses) placed at three, six, and eight targeted sites, respectively. Each defect, positioned within its respective cluster, completely blocks information propagation in that region, while causing lossless redistribution of information among the remaining clusters. The colorbar indicates of  $|\psi|$ , with red corresponding to high amplitude values and black to nearly zero ones.

performed a multi-tool analysis of both the overall properties of SG spectrum and the specific features of individual NEMs and provided sensitive indicators to distinguish between different types of them. Among other findings, we demonstrated that one particular type of states – compact localized states – respond in a highly symmetric and structured way to introducing random disorder, making them an interesting platform for quantum control.

Not to limit ourselves with only one fractal geometry, in the Supplemental Material, we generalized our findings to another structure: the negative Vicsek fractal, where vacancies (rather than the remaining lattice sites) form a fractal of rather low Hausdorff dimension ( $\simeq 1.46$ ), and next-nearest hoppings are allowed. The main goal to consider this

particular example was that its creation requires introducing a minimal number of defects as compared with structures like SG or the Sierpiński carpet, making its experimental realization easier. While most of the states in this geometry are ergodic, NEMs still emerge in certain parts of the spectrum. Besides, it demonstrates the emergence of non-ergodic multifractal states (NEMs) in a system with beyond nearest-neighbor kinetics [13] and large translationally invariant clean sub-domains.

We suggest that artificial fractal structures – systems that have already been created in a lab – are a natural platform to create and study multifractal states experimentally, which so far – to our knowledge – has been possible only in doped semiconductors [57] and yet remains an ongoing challenge. Our numerical results, particularly on the two-point density-density correlation function  $\mathcal{F}(\omega, E)$ , provide a direct method to distinguish NEMs using scanning probe microscopy techniques (recent research has also demonstrated applicability of similar methods in acoustic metamaterials [58] and photonic systems [40, 59]).

The signatures of multifractal states that we have analyzed here, lay a natural ground for further research. First of all, we have considered only single-particle quantum mechanics. Further studies could focus on how the observed phenomena change upon introducing interactions, potentially relating to such phenomena as many-body localization, Hilbert space fragmentation [21], and quantum scars [60, 61]. The demonstrated properties of compact localized states, also known for their ability to support dispersionless wave propagation [54, 62], can be deeper analyzed in connection with controlled information flow between targeted regions of the system, offering new approaches to quantum control.

## METHODS

### Singularity spectrum

The generalized fractal dimension  $D_q$  of eigenstates  $\psi_i$  with energy  $E$  is defined as [14]:

$$D_q(E) = \frac{1}{(1-q)\ln N} \ln \sum_{i=1}^N \sum_{r=1}^N |\psi_i(r)|^{2q} \delta(E - \lambda_i) \quad (3)$$

The information encoded in the fractal dimensions can be refined by analysing the singularity spectrum  $f(\alpha)$  [19, 63, 64], which, for each  $\alpha$ , can be regarded as a fractal dimension of the set of points, where the wavefunction intensity is  $|\psi|^2 \sim N^{-\alpha}$  [2]. It can be obtained as the Legendre transform of the mass exponent dimensions  $\tau_q \equiv (q-1)D_q$ :

$$\begin{aligned} \alpha_q &= \frac{d\tau_q}{dq}, & q &= \frac{df}{d\alpha} \\ f(\alpha_q) &= \alpha_q q - \tau_q. \end{aligned} \quad (4)$$

The maximal value of this function is always  $f(\alpha_{max}) = 1$ , and it obeys the relation:  $f(1+\alpha) = f(1-\alpha) + \alpha$  [65]. For ergodic states, the singularity spectrum shows a narrow distribution around the maximum, converging to a  $\delta(\alpha - 1)$  in the limit of ideal extended states, as it happens, for example, in the case of Gaussian Orthogonal Ensemble. For ideally localized states,  $f(\alpha)$  has its support in just two points,  $\alpha = 0$  with  $f(0) = 0$ , and  $\alpha = \infty$  with  $f(\infty) = 1$ . For multifractal states, a smooth parabolic spectrum is typically expected, which should be independent of the size of the system. However, the degree of multifractality can significantly influence the result, affecting both convexity of the spectrum and its support range. Properties of the singularity spectrum can be analyzed in more detail through extrapolation to the thermodynamic limit [27, 66] or using graphical methods [67], but we do not employ these approaches here.

### Two-eigenstates correlator

Following Berezinskii and Gorkov [68], we define the two-point density correlator at energy  $E$  for an arbitrary pair of points  $(r, r')$  as:

$$\rho_E(r)\rho_{E+\omega}(r') = \frac{1}{n(E)} \sum_{i,j} |\psi_i(r)|^2 |\psi_j(r')|^2 \delta(E - \lambda_i) \delta(E - \lambda_j + \omega), \quad (5)$$

where  $n(E)$  is the density of states, and  $\omega$  is the energy difference between two states. In the case of extended states, the corresponding wavefunctions are spread over all  $N$  sites of the system (here, we always deal with fractals

embedded in  $2d$  space), and each term in the sum scales as  $N^{-2}$ , vanishing in the limit  $N \rightarrow \infty$ . In the localized case, the wavefunctions have their support in a finite volume proportional to square of the characteristic localization length, and the density correlator is dominated – apart from a nonsingular contribution – by a pole singularity:

$$\rho_E(r)\rho_{E+\omega}(r') \sim A_E(r-r')\delta(\omega), \quad (6)$$

where the spectral function

$$A_E(r-r') = \frac{1}{n(E)} \sum_i |\psi_i(r)|^2 |\psi_i(r')|^2 \delta(E - \lambda_i) \quad (7)$$

is directly related to the number of sites in the support of the considered quantum states and can be linked to the fractal dimension  $D_q$ , see Eq.(3).

This probe has been widely used to study translationally invariant disordered quantum systems [45, 64]. For the fractal geometries that lack translational invariance, it is more handy to work with the spectral correlation function  $\mathcal{F}(\omega, E)$  defined as:

$$\mathcal{F}(\omega, E) = \frac{N \sum_r \sum_{i,j} |\psi_i(r)|^2 |\psi_j(r)|^2 \delta\left(E - \lambda_i - \frac{\omega}{2}\right) \delta\left(E - \lambda_j + \frac{\omega}{2}\right)}{\sum_{i,j} \delta\left(E - \lambda_i - \frac{\omega}{2}\right) \delta\left(E - \lambda_j + \frac{\omega}{2}\right)}. \quad (8)$$

This function effectively quantifies overlaps between eigenstates separated by energy  $\omega$ . To perform numerical simulations, we smeared the  $\delta$ -functions with Gaussian distributions.

For ideal extended states, such as those described by the Gaussian Orthogonal Ensemble (GOE), the correlator  $\mathcal{F}(\omega, E) = 1$  across the entire spectral range, and the eigenfunctions are completely uncorrelated [45, 53]. Analysing more realistic scenarios, such as typical metals, a broad plateau appears at  $\mathcal{F}(\omega, E) > 1$ , and its height increases as the states become more localized. As the separation between eigenstates grows, the plateau region becomes bounded by a cutoff energy – the Thouless energy  $E_{Th}$  – at the scale of the lattice spacing [69, 70], beyond which the system returns to the uncorrelated regime. For a multifractal state, the plateau is present only within a narrow energy interval, and the Thouless energy shrinks to zero in the thermodynamic limit. In this case, the uncorrelated limit at large values of  $\omega$  is preceded by power-law decay  $\mathcal{F}(\omega, E) \sim (\omega/E_{Th})^{-\mu}$  in the intermediate range of energies, where  $\mu$  is the critical exponent [69]. With system size  $N$ , wavefunction amplitudes on each site scale as  $N^{-D_2}$ . Consequently, the height of the plateau at low energies scales as  $\mathcal{F}(0, E) \propto N^{1-D_2}$ . For NEMs, this implies that  $\mathcal{F}(\omega, E)$  for different system sizes  $N$  should collapse onto a single curve when the vertical axis is rescaled by  $N^{1-D_2}$ .

## AVAILABILITY OF DATA

Data are available from the corresponding author upon reasonable request.

## ACKNOWLEDGEMENTS

We are grateful to C. Morais Smith, M.R. Slot, A. Moustaj, M. Conte and Y. in 't Veld for insightful discussions. We would also like to thank I.M. Khaymovich for valuable correspondence. This work was supported by the European Research Council (ERC) under the European Union's Horizon 2020 research and innovation program, grant agreement 854843-FASTCORR.

---

[1] P. W. Anderson, Absence of diffusion in certain random lattices, *Phys. Rev.* **109**, 1492 (1958).  
[2] F. Evers and A. D. Mirlin, Anderson transitions, *Rev. Mod. Phys.* **80**, 1355 (2008).  
[3] C. Castellani and L. Peliti, Multifractal wavefunction at the localisation threshold, *Journal of physics A: mathematical and general* **19**, L429 (1986).  
[4] U. Frisch, Fully developed turbulence and intermittency, *Annals of the New York Academy of Sciences* **357**, 359 (1980).  
[5] F. Gerges, X. Geng, H. Nassif, and M. C. Boufadel, Anisotropic Multifractal Scaling of Mount Lebanon Topography: Approximate Conditioning, *Fractals* **29**, 2150112-3222 (2021).

[6] F. Schmitt, D. Schertzer, and S. Lovejoy, Multifractal fluctuations in finance, *International Journal of Theoretical and Applied Finance* **03**, 361 (2000), <https://doi.org/10.1142/S0219024900000206>.

[7] P. C. Ivanov, L. A. N. Amaral, A. L. Goldberger, S. Havlin, M. G. Rosenblum, Z. R. Struzik, and H. E. Stanley, Multifractality in human heartbeat dynamics, *Nature* **399**, 461 (1999).

[8] Y. Long, Y. Chen, and Y. Li, Multifractal scaling analyses of the spatial diffusion pattern of covid-19 pandemic in chinese mainland, *Humanities and Social Sciences Communications* **10**, 636 (2023).

[9] Z. Wang, F. Zhang, M. Ren, and D. Gao, A new multifractal-based deep learning model for text mining, *Information Processing & Management* **61**, 103561 (2024).

[10] X. Yu, D. Zhang, T. Zhu, and X. Jiang, Novel hybrid multi-head self-attention and multifractal algorithm for non-stationary time series prediction, *Information Sciences* **613**, 541 (2022).

[11] B. Simon, Operators with singular continuous spectrum: I. general operators, *Annals of Mathematics* **141**, 131 (1995).

[12] S. Jitomirskaya and B. Simon, Operators with singular continuous spectrum: III. almost periodic schrödinger operators, *Communications in Mathematical Physics* **165**, 201 (1994).

[13] A. Avila, S. Jitomirskaya, and C. A. Marx, Spectral theory of extended harper's model and a question by erdős and szekeres, *Inventiones mathematicae* **210**, 283 (2017).

[14] A. Rodriguez, L. J. Vasquez, K. Slevin, and R. A. Römer, Multifractal finite-size scaling and universality at the anderson transition, *Phys. Rev. B* **84**, 134209 (2011).

[15] R. Ketzmerick, G. Petschel, and T. Geisel, Slow decay of temporal correlations in quantum systems with cantor spectra, *Phys. Rev. Lett.* **69**, 695 (1992).

[16] X.-Y. Xu, X.-W. Wang, D.-Y. Chen, C. M. Smith, and X.-M. Jin, Quantum transport in fractal networks, *Nature Photonics* **15**, 703 (2021).

[17] K. Agarwal, S. Gopalakrishnan, M. Knap, M. Müller, and E. Demler, Anomalous diffusion and griffiths effects near the many-body localization transition, *Phys. Rev. Lett.* **114**, 160401 (2015).

[18] T. Orito and K.-I. Imura, Multifractality and fock-space localization in many-body localized states: One-particle density matrix perspective, *Phys. Rev. B* **103**, 214206 (2021).

[19] B. Jäck, F. Zinser, E. J. König, S. N. P. Wissing, A. B. Schmidt, M. Donath, K. Kern, and C. R. Ast, Visualizing the multifractal wave functions of a disordered two-dimensional electron gas, *Phys. Rev. Res.* **3**, 013022 (2021).

[20] N. Macé, F. Alet, and N. Laflorencie, Multifractal scalings across the many-body localization transition, *Phys. Rev. Lett.* **123**, 180601 (2019).

[21] F. Pietracaprina and N. Laflorencie, Hilbert-space fragmentation, multifractality, and many-body localization, *Annals of Physics* **435**, 168502 (2021), special Issue on Localisation 2020.

[22] M. V. Feigel'man, L. B. Ioffe, V. E. Kravtsov, and E. A. Yuzbashyan, Eigenfunction fractality and pseudogap state near the superconductor-insulator transition, *Phys. Rev. Lett.* **98**, 027001 (2007).

[23] C. Rubio-Verdú, A. M. García-García, H. Ryu, D.-J. Choi, J. Zaldívar, S. Tang, B. Fan, Z.-X. Shen, S.-K. Mo, J. I. Pascual, and M. M. Ugeda, Visualization of multifractal superconductivity in a two-dimensional transition metal dichalcogenide in the weak-disorder regime, *Nano Letters* **20**, 5111 (2020), pMID: 32463696.

[24] S. Aubry and G. André, Analyticity breaking and anderson localization in incommensurate lattices, *Proceedings, VIII International Colloquium on Group-Theoretical Methods in Physics* **3** (1980).

[25] T. Shimasaki, M. Prichard, H. E. Kondakci, J. E. Pagett, Y. Bai, P. Dotti, A. Cao, A. R. Dardia, T.-C. Lu, T. Grover, and D. M. Weld, Anomalous localization in a kicked quasicrystal, *Nature Physics* **20**, 409 (2024).

[26] J. T. Edwards and D. J. Thouless, Numerical studies of localization in disordered systems, *Journal of Physics C: Solid State Physics* **5**, 807 (1972).

[27] A. De Luca, B. L. Altshuler, V. E. Kravtsov, and A. Scardicchio, Anderson localization on the bethe lattice: Nonergodicity of extended states, *Phys. Rev. Lett.* **113**, 046806 (2014).

[28] J. Arenz and M. R. Zirnbauer, Wegner model on a tree graph: U(1) symmetry breaking and a non-standard phase of disordered electronic matter (2023), arXiv:2305.00243 [cond-mat.dis-nn].

[29] B. B. Mandelbrot, *The Fractal Geometry of Nature*, revised edition ed. (W.H. Freeman, San Francisco, 1982).

[30] A. A. Iliasov, M. I. Katsnelson, and S. Yuan, Hall conductivity of a sierpiński carpet, *Phys. Rev. B* **101**, 045413 (2020).

[31] R. Canyellas, C. Liu, R. Arouca, L. Eek, G. Wang, Y. Yin, D. Guan, Y. Li, S. Wang, H. Zheng, C. Liu, J. Jia, and C. M. Smith, Topological edge and corner states in bi fractals on insb (2023), arXiv:2309.09860 [cond-mat.mes-hall].

[32] Q. Yao, X. Yang, A. A. Iliasov, M. I. Katsnelson, and S. Yuan, Energy-level statistics in planar fractal tight-binding models, *Phys. Rev. B* **107**, 115424 (2023).

[33] T. Westerhout, E. van Veen, M. I. Katsnelson, and S. Yuan, Plasmon confinement in fractal quantum systems, *Phys. Rev. B* **97**, 205434 (2018).

[34] E. van Veen, S. Yuan, M. I. Katsnelson, M. Polini, and A. Tomadin, Quantum transport in sierpinski carpets, *Phys. Rev. B* **93**, 115428 (2016).

[35] S. N. Kempkes, M. R. Slot, S. E. Freeney, S. J. M. Zevenhuizen, D. Vanmaekelbergh, I. Swart, and C. M. Smith, Design and characterization of electrons in a fractal geometry, *Nature Physics* **15**, 127 (2019).

[36] K. Mondal, S. Ganguly, and S. K. Maiti, Possible route to efficient thermoelectric applications in a driven fractal network, *Scientific Reports* **11**, 17049 (2021).

[37] M. N. Ivaki, I. Sahlberg, K. Pöyhönen, and T. Ojanen, Topological random fractals, *Communications Physics* **5**, 327 (2022).

[38] M. Brzezińska, A. M. Cook, and T. Neupert, Topology in the sierpiński-hofstadter problem, *Phys. Rev. B* **98**, 205116 (2018).

[39] A. A. Iliasov, M. I. Katsnelson, and A. A. Bagrov, Strong enhancement of superconductivity on finitely ramified fractal lattices (2024), arXiv:2310.11497 [cond-mat.supr-con].

[40] T. Biesenthal, L. J. Maczewsky, Z. Yang, M. Kremer, M. Segev, A. Szameit, and M. Heinrich, Fractal photonic topological insulators, *Science* **376**, 1114 (2022), <https://www.science.org/doi/pdf/10.1126/science.abm2842>.

[41] E. H. Lieb, Two theorems on the hubbard model, *Phys. Rev. Lett.* **62**, 1201 (1989).

[42] M. Röntgen, C. V. Morfonios, I. Brouzos, F. K. Diakonos, and P. Schmelcher, Quantum network transfer and storage with compact localized states induced by local symmetries, *Phys. Rev. Lett.* **123**, 080504 (2019).

[43] A. A. Khajetoorians, D. Wegner, A. F. Otte, and I. Swart, Creating designer quantum states of matter atom-by-atom, *Nature Reviews Physics* **1**, 703 (2019).

[44] E. Sierda, X. Huang, D. I. Badrtdinov, B. Kiraly, E. J. Knol, G. C. Groenenboom, M. I. Katsnelson, M. Rösner, D. Wegner, and A. A. Khajetoorians, Quantum simulator to emulate lower-dimensional molecular structure, *Science* **380**, 1048 (2023), <https://www.science.org/doi/pdf/10.1126/science.adf2685>.

[45] E. Cuevas and V. E. Kravtsov, Two-eigenfunction correlation in a multifractal metal and insulator, *Phys. Rev. B* **76**, 235119 (2007).

[46] N. C. Murphy, R. Wortis, and W. A. Atkinson, Generalized inverse participation ratio as a possible measure of localization for interacting systems, *Phys. Rev. B* **83**, 184206 (2011).

[47] Q. Dai, Z. Lu, and Z. Xu, Emergence of multifractality through cascadelike transitions in a mosaic interpolating aubry-andré-fibonacci chain, *Phys. Rev. B* **108**, 144207 (2023).

[48] G. De Tomasi and I. M. Khaymovich, Multifractality meets entanglement: Relation for nonergodic extended states, *Phys. Rev. Lett.* **124**, 200602 (2020).

[49] A. D. Mirlin and Y. V. Fyodorov, Distribution of local densities of states, order parameter function, and critical behavior near the anderson transition, *Phys. Rev. Lett.* **72**, 526 (1994).

[50] M. Conte, V. Zampronio, M. Röntgen, and C. M. Smith, The fractal-lattice hubbard model (2023), arXiv:2310.07813 [cond-mat.str-el].

[51] S. Fischer, M. van Hooft, T. van der Meijden, C. M. Smith, L. Fritz, and M. Fremling, Robustness of chiral edge modes in fractal-like lattices below two dimensions: A case study, *Phys. Rev. Res.* **3**, 043103 (2021).

[52] Y. V. Fyodorov and A. D. Mirlin, Scaling properties of localization in random band matrices: A  $\sigma$ -model approach, *Phys. Rev. Lett.* **67**, 2405 (1991).

[53] L. F. Cugliandolo, G. Schehr, M. Tarzia, and D. Venturelli, Multifractal phase in the weighted adjacency matrices of random erdős-rényi graphs (2024), arXiv:2404.06931 [cond-mat.dis-nn].

[54] N. Lazarides and G. Tsironis, Compact localized states in engineered flat-band pt metamaterials, *Scientific Reports* **9**, 4904 (2019).

[55] W. Jolie, T.-C. Hung, L. Niggli, B. Verlhac, N. Hauptmann, D. Wegner, and A. A. Khajetoorians, Creating tunable quantum corrals on a rashba surface alloy, *ACS Nano* **16**, 4876 (2022).

[56] A. A. Iliasov, M. I. Katsnelson, and S. Yuan, Power-law energy level spacing distributions in fractals, *Phys. Rev. B* **99**, 075402 (2019).

[57] A. Richardella, P. Roushan, S. Mack, B. Zhou, D. A. Huse, D. D. Awschalom, and A. Yazdani, Visualizing critical correlations near the metal-insulator transition in  $\text{Ga}(1-x)\text{Mn}(x)\text{As}$ , *Science* **327**, 665 (2010).

[58] S. Zheng, X. Man, Z.-L. Kong, Z.-K. Lin, G. Duan, N. Chen, D. Yu, J.-H. Jiang, and B. Xia, Observation of fractal higher-order topological states in acoustic metamaterials, *Science Bulletin* **67**, 2069 (2022).

[59] M. Li, C. Li, L. Yan, Q. Li, Q. Gong, and Y. Li, Fractal photonic anomalous floquet topological insulators to generate multiple quantum chiral edge states, *Light: Science & Applications* **12**, 262 (2023).

[60] M. Serbyn, D. A. Abanin, and Z. Papić, Quantum many-body scars and weak breaking of ergodicity, *Nature Physics* **17**, 675 (2021).

[61] H.-R. Wang, D. Yuan, S.-Y. Zhang, Z. Wang, D.-L. Deng, and L.-M. Duan, Embedding quantum many-body scars into decoherence-free subspaces, *Phys. Rev. Lett.* **132**, 150401 (2024).

[62] M. Röntgen, M. Pyzh, C. V. Morfonios, N. E. Palaiodimopoulos, F. K. Diakonos, and P. Schmelcher, Latent symmetry induced degeneracies, *Phys. Rev. Lett.* **126**, 180601 (2021).

[63] A. Chhabra and R. V. Jensen, Direct determination of the  $f(\alpha)$  singularity spectrum, *Phys. Rev. Lett.* **62**, 1327 (1989).

[64] V. E. Kravtsov, I. M. Khaymovich, E. Cuevas, and M. Amini, A random matrix model with localization and ergodic transitions, *New Journal of Physics* **17**, 122002 (2015).

[65] A. D. Mirlin, Y. V. Fyodorov, A. Mildenberger, and F. Evers, Exact relations between multifractal exponents at the anderson transition, *Phys. Rev. Lett.* **97**, 046803 (2006).

[66] X. Deng, A. L. Burin, and I. M. Khaymovich, Anisotropy-mediated reentrant localization, *SciPost Phys.* **13**, 116 (2022).

[67] A. Kutlin and I. M. Khaymovich, Anatomy of the eigenstates distribution: A quest for a genuine multifractality, *SciPost Phys.* **16**, 008 (2024).

[68] V. Berezinskii and L. Gor'kov, On the theory of electrons localized in the field of defects, *Zh. Eksp. Teor. Fiz.* **77**, 2498 (1979).

[69] J. T. Chalker and G. J. Daniell, Scaling, diffusion, and the integer quantized hall effect, *Phys. Rev. Lett.* **61**, 593 (1988).

[70] J. Chalker, Scaling and eigenfunction correlations near a mobility edge, *Physica A: Statistical Mechanics and its Applications* **167**, 253 (1990).

## Supplementary material

### I. FURTHER CHARACTERIZATION OF REPRESENTATIVE EXTENDED, LOCALIZED, AND NON-ERGODIC MULTIFRACTAL STATES

#### A. Size-scaling and amplitude profiles

Multifractal properties can be deduced from scaling behavior with system size. In fractal structures like the Sierpiński Gasket, each generation grows by a fixed number of points to maintain self-similarity, which constrains the range of accessible system sizes within computational limits. Nonetheless, we can support our findings on multifractality by comparing the singularity spectra of the fifth and sixth generations and with the amplitude profiles of the studied cases – Fig. (S1) and Fig. (S2).

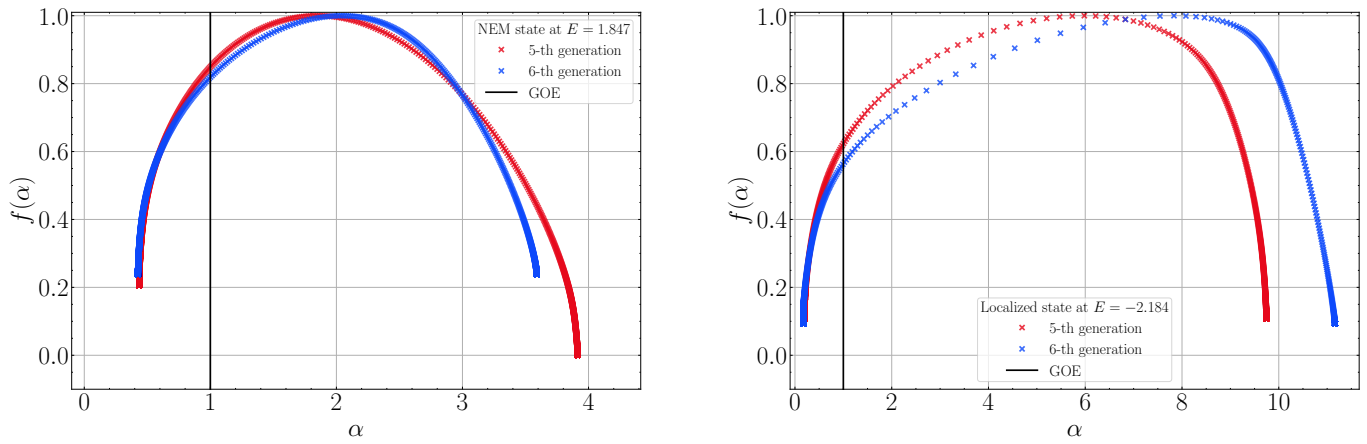


FIG. S1. Scaling of the singularity spectrum  $f(\alpha)$  for the NEM and localized states case studies discussed in the main text. The system sizes correspond to the fifth and sixth generations of the Sierpiński Gasket. On the left, the scaling of  $f(\alpha)$  for the NEM state at  $E = 1.847$ , shows great agreement between generations, confirming the genuine multifractal nature of the state. On the right, the scaling of  $f(\alpha)$  for the localized state at  $E = -2.184$  shows the effects of finite-size limitations, which prevent  $f(0) \rightarrow 0$ . In spite of that, a trend towards convergence is evident in successive generations, also with the function's apex shifting to higher  $\alpha$  values, consistent with the behavior of a rigorously localized state.

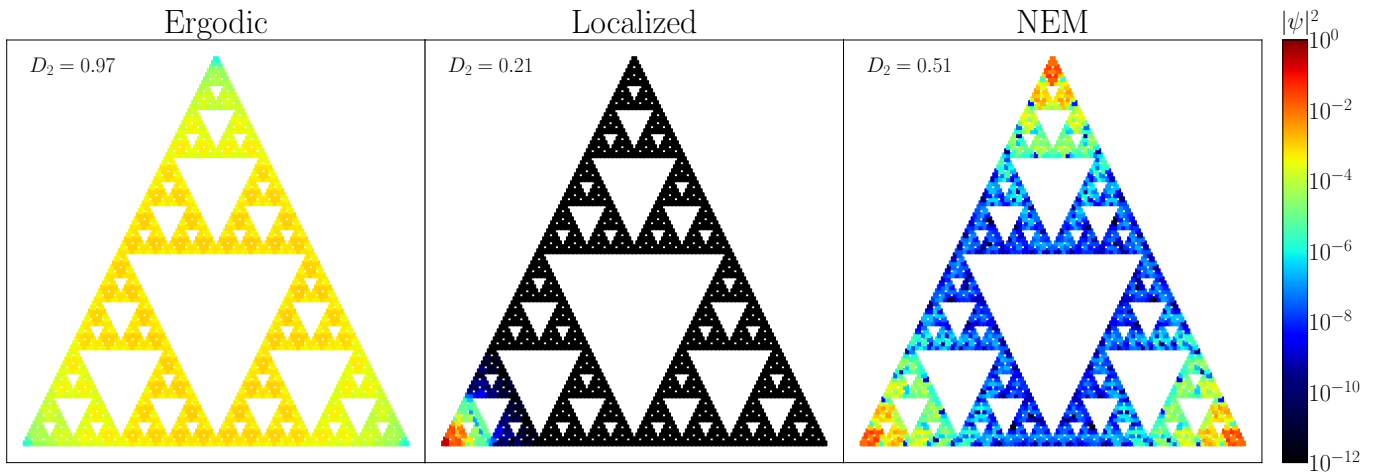


FIG. S2. Intensity profiles of ergodic, localized, and non-ergodic multifractal (NEM) states. Representative examples of intensity distributions are presented for an ergodic state (energy  $E = -3.666$ ), a localized state ( $E = -2.184$ ), and a NEM state ( $E = 1.847$ ). Red color represents high intensity, and black corresponds to negligibly small intensity. For the sake of simplicity, the defects that reshape the triangular lattice into a SG are shown as voids. In the ergodic phase, the intensity is homogeneously distributed across all sites, indicating delocalization. The localized state exhibits a strong concentration of intensity in a small region, in this case near the corner. The NEM state has a heterogeneous intensity profile with strong fluctuations that differs from either extended or localized states and repeating across all scales.

## II. DETAILS ON CLSS

### A. Fractal dimensions and amplitude profiles of CLSs

In the main text, we presented the singularity spectrum for the CLSs. Here, we further investigate a characteristic feature of these spectra: the broad horizontal part, which is usually associated with faster-than-polynomial decay [1] and that can also be observed in monofractal states. To understand this property in detail, we plot the fractal dimension  $D_q$  as a function of moment order  $q$  for the analysed CLSs, as shown in Fig. (S3). In Fig. (S4), the corresponding amplitude profiles.

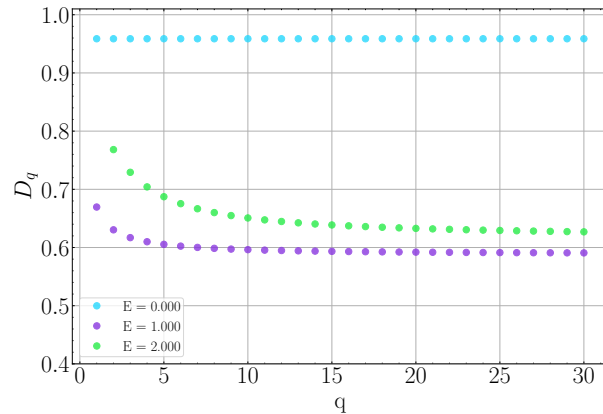


FIG. S3. Fractal dimension  $D_q$  as a function of moment order  $q$  for three representative of CLSs. The cyan curve for  $E = 0.000$  maintains a constant  $D_q$  for any  $q$ . Given the high value of the fractal dimension and in light of the localized characteristics of its singularity spectrum, we conclude that this state represents an extensive set of localized states. In contrast, the curves at  $E = 1.000$  (purple) and  $E = 2.000$  (green) exhibit a non-trivial dependence on  $q$ , signaling the presence of more complex localized structures.

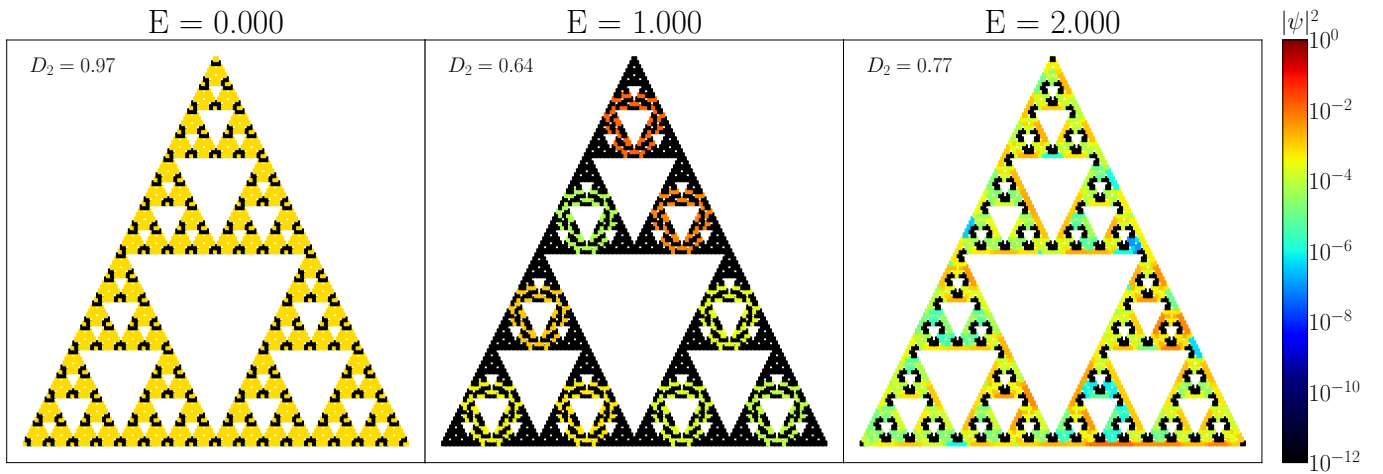


FIG. S4. Intensity profiles for compact localized states. We show three distinct types of compact localized states at integer energy values:  $E = 0.000$ ,  $E = 1.000$ , and  $E = 2.000$ . These formations arise from interference between resonant groups of sites, which leads to the confinement of intensity in compact regions [2].

### B. Robustness of CLSs against randomly displaced defects

In Fig. (S5), we show the number of CLSs at each energy level as a function of the number of randomly introduced defects. While one might expect that adding defects would disrupt the self-similar structure of the fractal, lift degeneracy of the energy level, and destroy some of CLSs, quite opposite behavior is observed. By adding random defects, one can even enhance quantum interference patterns, making CLSs more degenerate, as observed in the increasing number of states at  $E = 1.000$  level. It is possible to check that all these states are indeed compact localized. Fig. (S6) displays the intensity profile of one of CLSs at  $E = 1.000$  before and after adding random defects.

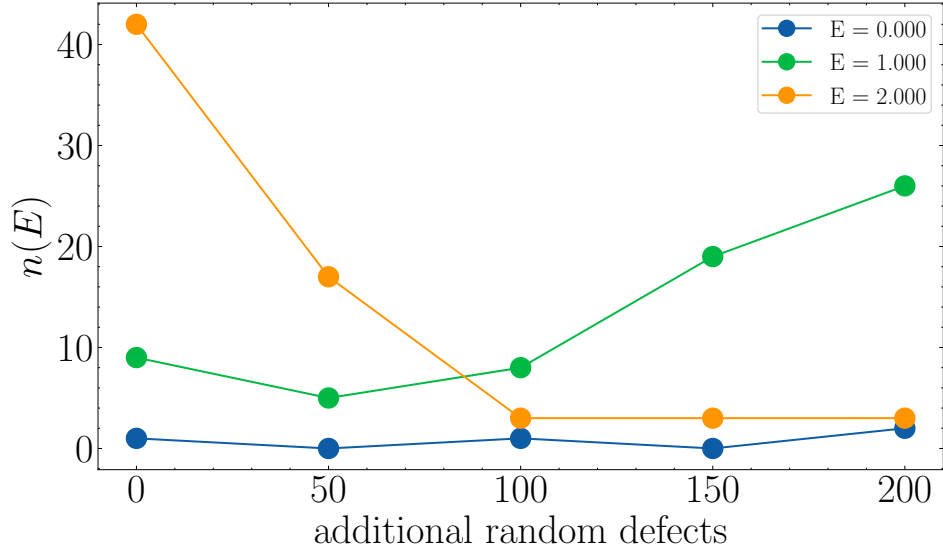


FIG. S5. Change in the number of compact localized states at  $E = 0.000, 1.000$ , and  $2.000$  when additional random defects are introduced in the Sierpiński Gasket.

### III. OTHER EXAMPLES OF NEMS

In this section, we show data for different types of multifractality. Fig. (S7) shows the singularity spectra for NEMs of different energy levels  $E$ , similarly to Fig.3 from the main text. Fig. (S8) shows their corresponding intensity

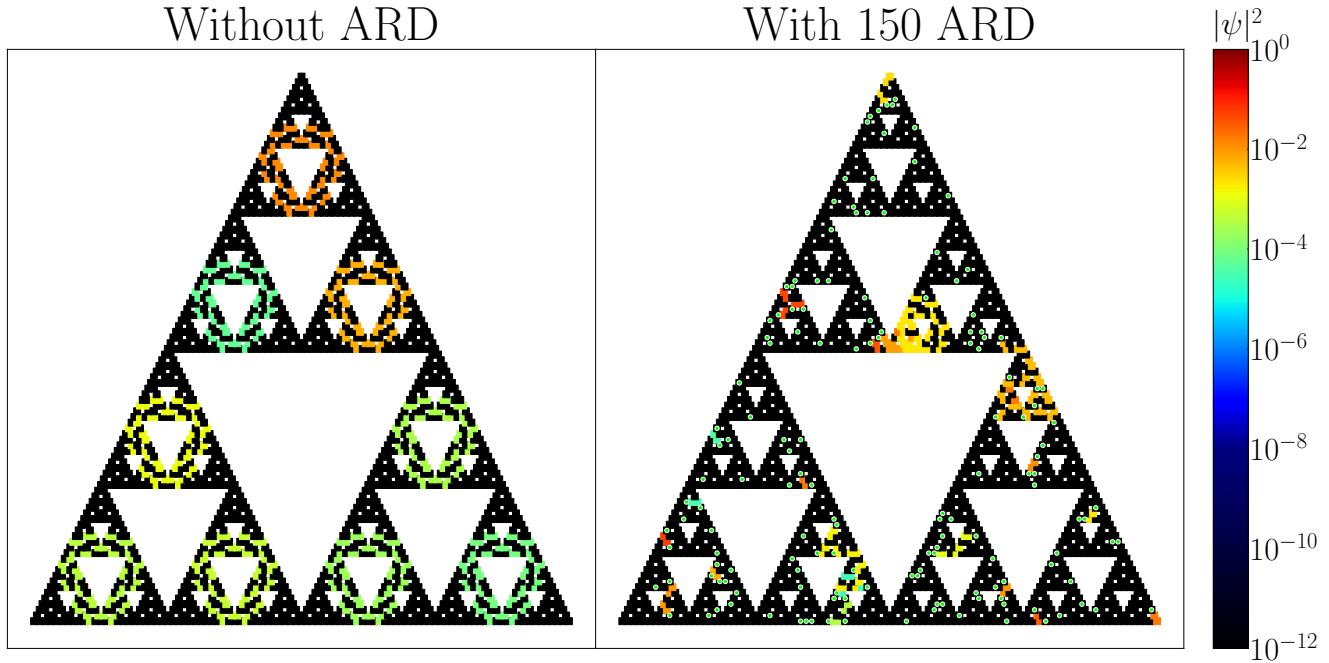


FIG. S6. Intensity profiles for one of the CLSs with energy  $E = 1.000$ . The left panel shows the profile without additional random defects (ARD), while the right panel the profile with 150 additional random defects. The ARD are highlighted by lime circles. The introduction of these additional defects generates new quantum interference patterns, and the intensity is redistributed primarily towards the lower hierarchical levels of the SG structure.

profiles. In Fig. Fig. (S9), for a few examples, it is demonstrated that spectral density-density correlation functions of NEMs can behave in rather different ways, but obey roughly the same pattern – narrow plateau followed by smooth fall-off, and the subsequent oscillations and revivals.

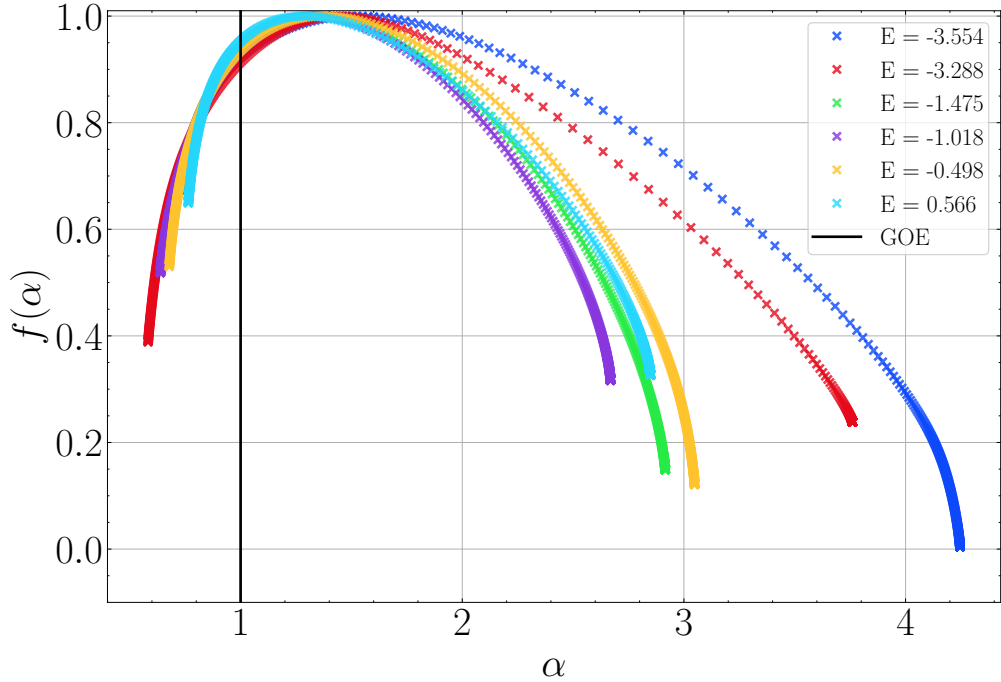


FIG. S7. Singularity spectrum  $f(\alpha)$  of states with different strength of multifractality. Each curve corresponds to a NEM state, having the typical convex shape and a shift of the spectrum apex from the GOE reference (solid black line). The bending and the termination of the right branch of each singularity spectrum reflect different levels of fluctuations in the state structure, serving as quantitative marker for the level of multifractality.

#### IV. NEGATIVE VICSEK FRACTAL

##### A. The model

In this section, we explore emergence of NEMs in another type of fractal that can potentially be easier to fabricate than SG – the negative Vicsek (NV) fractal – as it requires way fewer defects to be placed in a controllable manner. The starting point is a uniform square lattice  $\mathcal{S}$  of  $N$  sites. Then, unlike in the SG case, we retain sites corresponding to voids of the fractal and remove all other sites, see Figs. S10 and S11. We denote the set of indices of the removed sites as  $\mathcal{B} \subset \mathcal{S}$ .

As in the SG case, each defect at position  $r_i$  is modeled by a delta-peaked potential,  $V_i = V, \delta(r - r_i)$ , with strength  $V$  much larger than other energy scale in the system. However, in the NV model, we also account for next-nearest neighbor interactions, denoted by  $t'$ . These additional couplings are fundamental, as they maintain connectivity between otherwise isolated regions of the fractal. The hoppings between defects and the regular sites are weak. The corresponding Hamiltonian reads:

$$H = \sum_{\substack{\langle i,j \rangle \\ i,j \notin \mathcal{B}}} t c_i^\dagger c_j + \sum_{\substack{\langle\langle i,j \rangle\rangle \\ i,j \notin \mathcal{B}}} t' c_i^\dagger c_j + \sum_{i \in \mathcal{B}} V c_i^\dagger c_i + \sum_{\substack{\langle i,j \rangle \\ i \in \mathcal{B}}} \bar{t} c_i^\dagger c_j + \sum_{\substack{\langle\langle i,j \rangle\rangle \\ i \in \mathcal{B}}} \bar{t}' c_i^\dagger c_j + h.c. \quad (1)$$

Here, single brackets denote summations over the nearest neighbors, and the double brackets – over the next-nearest neighbors.

##### B. Fractal dimensions of states for the negative Vicsek lattice

In Fig. (S12), we present the fractal dimensions of states in the energy spectrum of the fourth generation of the NV fractal. The full set of eigenstates and eigenvalues is obtained through exact diagonalization of (1) with open boundary conditions. The parameters are set as  $t = t' = 1$ ,  $\bar{t} = \bar{t}' = 10^{-9}$ ,  $V = 10^4$ .

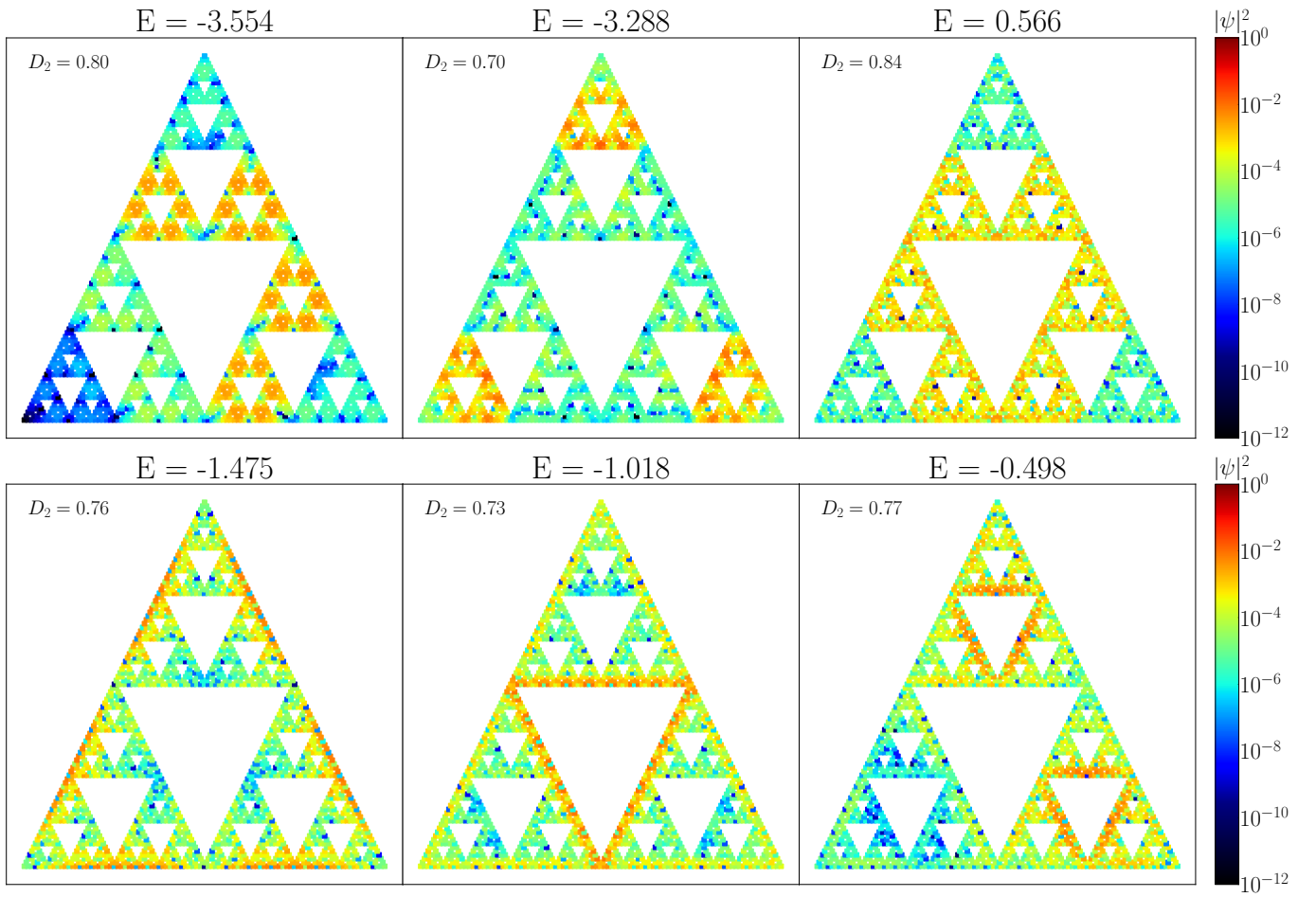


FIG. S8. Intensity profiles of NEMs with different singularity spectra. The first row: NEM states resembling bulk and corner modes. The second row: NEM states resembling edge modes. Such non-genuine NEM states are composed out of “pieces of multifractals” and may display properties of either insulators or metals [3].

---

[1] W. Tang and I. M. Khaymovich, Non-ergodic delocalized phase with poisson level statistics, *Quantum* **6**, 733 (2022).  
 [2] E. H. Lieb, Two theorems on the hubbard model, *Phys. Rev. Lett.* **62**, 1201 (1989).  
 [3] E. Cuevas and V. E. Kravtsov, Two-eigenfunction correlation in a multifractal metal and insulator, *Phys. Rev. B* **76**, 235119 (2007).

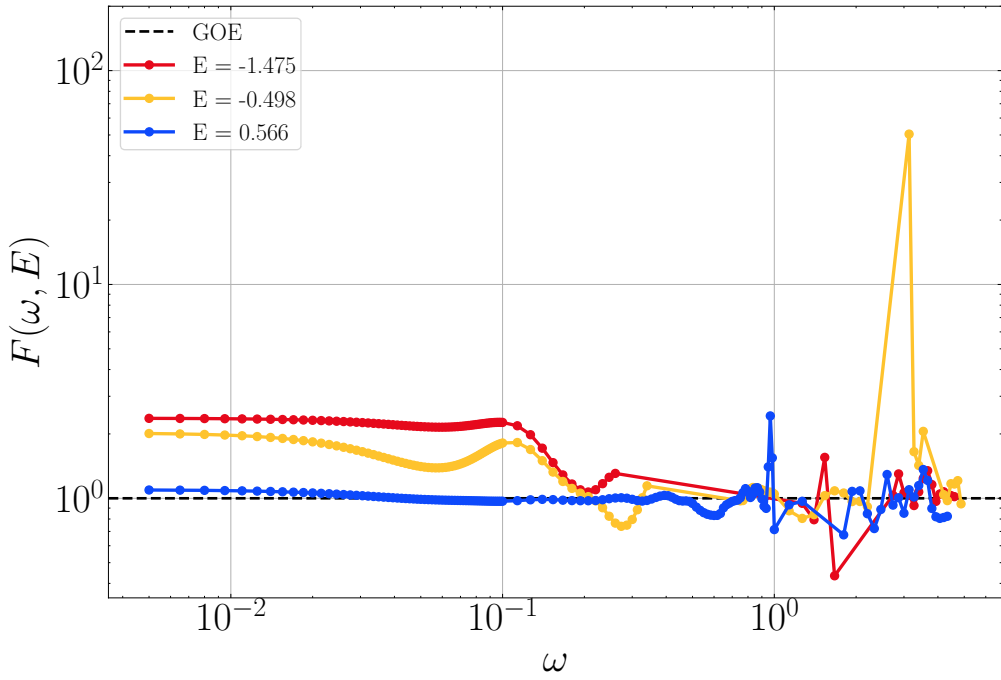


FIG. S9. Frequency correlator  $\mathcal{F}(\omega, E)$  for three distinct types of NEM states. Each state reveals unique characteristics in plateau width, slope behavior, and revival patterns. Lines are guide to eye.

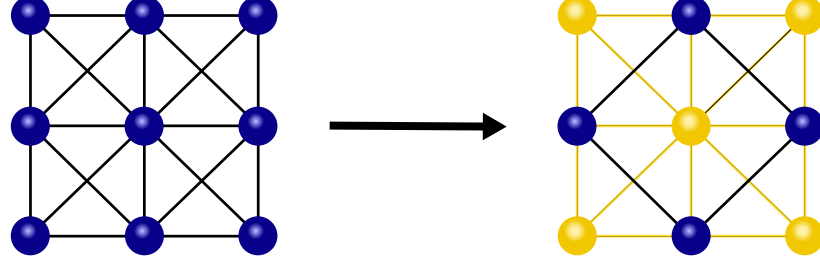


FIG. S10. Transformation of a minimal square lattice into the first-generation negative Vicsek fractal. Next-to-nearest hoppings are required to keep the lattice connected.

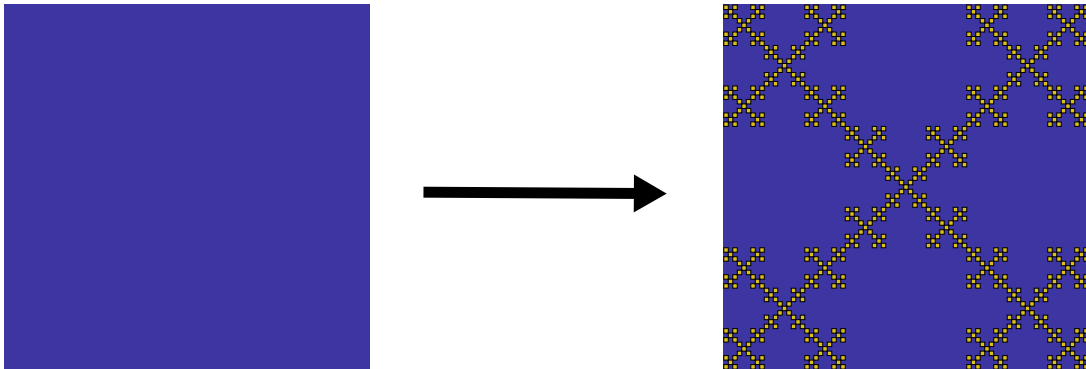


FIG. S11. Transformation of a square lattice into the fourth-generation Vicsek saltire fractal. The final structure emerges from successive iterations of the elementary transformation, where lattice sites belonging to subset  $\mathcal{B}$  are progressively replaced by defects. The resulting fractal is characterized by patching large regions of intact lattice without defects and regions with intricate defect patterns.

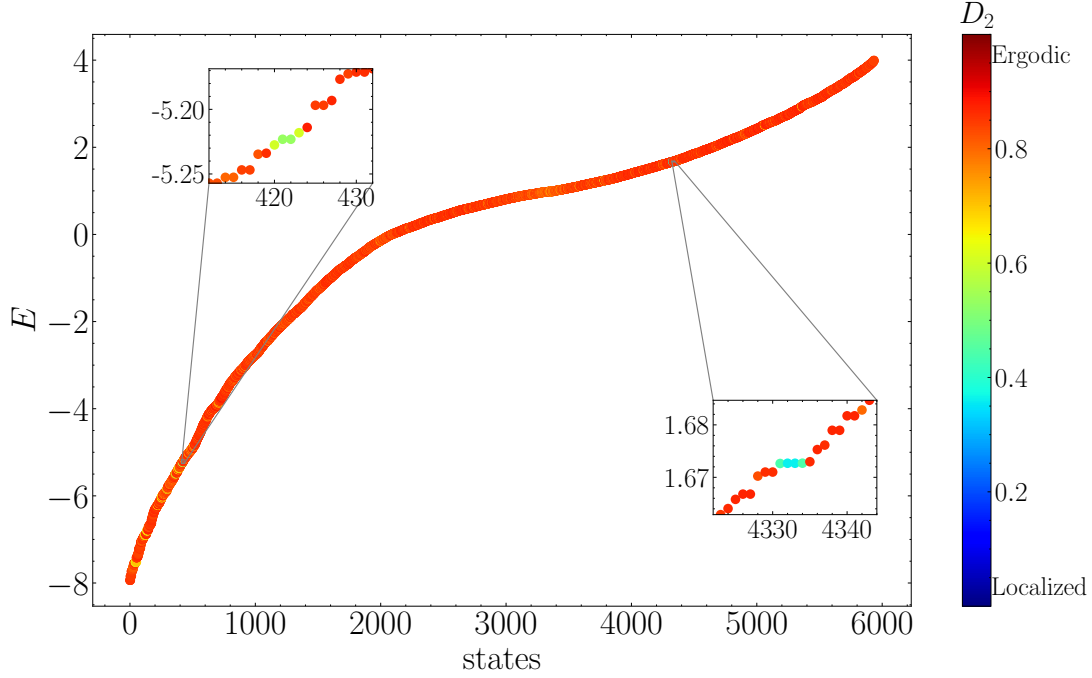


FIG. S12. Energy spectrum of the single-particle tight-binding model on the fourth generation of the negative Vicsek fractal. The color bar represents fractal dimension  $D_2$  of each eigenstate, ranging from localized (blue) to ergodic (red). Due to the large clean regions that are intact by deformations, formation of NEMs is inhibited, leaving most of the states ergodic. However, the fractal still enables the emergence of NEMs in certain parts of the energy spectrum, with about 8% of the states having fractal dimension  $D_2 \in (0.2, 0.8)$ .